pubs.acs.org/Biomac

Article

Dendrimer-Peptide Conjugates for Effective Blockade of the Interactions between SARS-CoV-2 Spike Protein and Human ACE2 Receptor

Woo-jin Jeong,[#] Jiyoon Bu,[#] Philip Mickel, Yanxiao Han, Piper A Rawding, Jianxin Wang, Hanbit Kang, Heejoo Hong,* Petr Král,* and Seungpyo Hong*

Cite This: *Biomacromolecules* 2023, 24, 141−149

Read Online

ACCESS | Metrics & More | Article Recommendations | Supporting Information

ABSTRACT: The coronavirus disease 2019 (COVID-19) pandemic has threatened the stability of global healthcare, which is becoming an endemic issue. Despite the development of various treatment strategies to fight COVID-19, the currently available treatment options have shown varied efficacy. Herein, we have developed an avidity-based SARS-CoV-2 antagonist using dendrimer-peptide conjugates (DPCs) for effective COVID-19 treatment. Two different peptide fragments obtained from angiotensin-converting enzyme 2 (ACE2) were integrated into a single sequence, followed by the conjugation to poly(amidoamine) (PAMAM) dendrimers. We hypothesized that the strong multivalent binding avidity endowed by dendrimers would help peptides effectively block the interaction between SARS-CoV-2 and ACE2, and this antagonist effect would be dependent upon the generation (size) of the dendrimers. To assess this, binding kinetics of the DPCs prepared from generation 4 (G4) and G7 PAMAM dendrimers to spike protein of SARS-CoV-2 were quantitatively measured using surface plasmon resonance. The larger dendrimer-based DPCs exhibited significantly enhanced binding strength by 3 orders of magnitude compared to the free peptides, whereas the smaller one showed a 12.8-fold increase only. An *in vitro* assay using SARS-CoV-2-mimicking microbeads also showed the improved SARS-CoV-2 blockade efficiency of the G7-peptide conjugates compared to G4. In addition, the interaction between the DPCs and SARS-CoV-2 was analyzed using molecular dynamics (MD) simulation, providing an insight into how the dendrimer-mediated multivalent binding effect can enhance the SARS-CoV-2 blockade. Our findings demonstrate that the DPCs having strong binding to SARS-CoV-2 effectively block the interaction between ACE2 and SARS-CoV-2, providing a potential as a high-affinity drug delivery system to direct anti-COVID payloads to the virus.

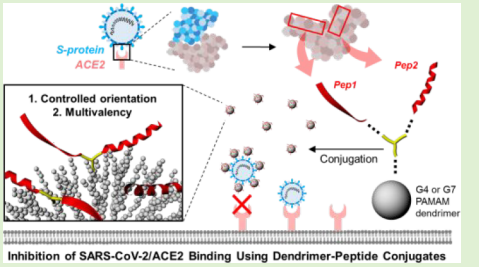

INTRODUCTION

Increasing changes in our society and environment have resulted in the emergence of novel and modified pathogens, resulting in significant global health challenges.[1] One such family of the emerging pathogens is Coronavirus (CoV) that is characterized by its high prevalence and distribution, genetic diversity, and rapid evolution.[2] Since the 1970s, a series of CoV infections have been reported in domestic animals;[3] however, they were not considered highly pathogenic to humans until the outbreak of severe acute respiratory syndrome (SARS) in the early 2000s in China and Middle East respiratory syndrome (MERS) in the early 2010s in Middle Eastern countries.[4,5] In late December 2019, a new CoV infection, SARS-CoV-2, emerged in China and was named coronavirus disease (COVID-19).[2,6] SARS-CoV-2 is an enveloped, positive-sense, and single-stranded RNA (+ssRNA) virus that belongs to the group of β-coronavirus (β-CoV), similar to both SARS and MERS; these viruses can infect mammals and jump species barriers, resulting in animal-to-human transmission. A full-length genome sequence has revealed that the SARS-CoV-2 is closely related with the other β-COV members, sharing ~80% and ~50% sequence identities with SARS-CoV-1 and MERS-CoV, respectively.[7] Although the clinical features of COVID-19 patients were described shortly after the emergence of the disease, no effective treatment was available. As a result, the World Health Organization (WHO) declared COVID-19 a global pandemic due to its high transmissibility and severity.[8−10] Since the beginning of the pandemic, mitigation strategies have included social distancing, wearing facemasks, travel restrictions, stay-at-home orders, and viral testing. With the successful development, evaluation, and production of multiple vaccines, however, vaccination has helped reduce the spread of COVID-19.[11] However, as of 20 January 2022, there have been 5.57 million confirmed deaths and 342 million confirmed cases of infection with SARS-CoV-2.[12]

Received: August 17, 2022
Revised: December 1, 2022
Published: December 23, 2022

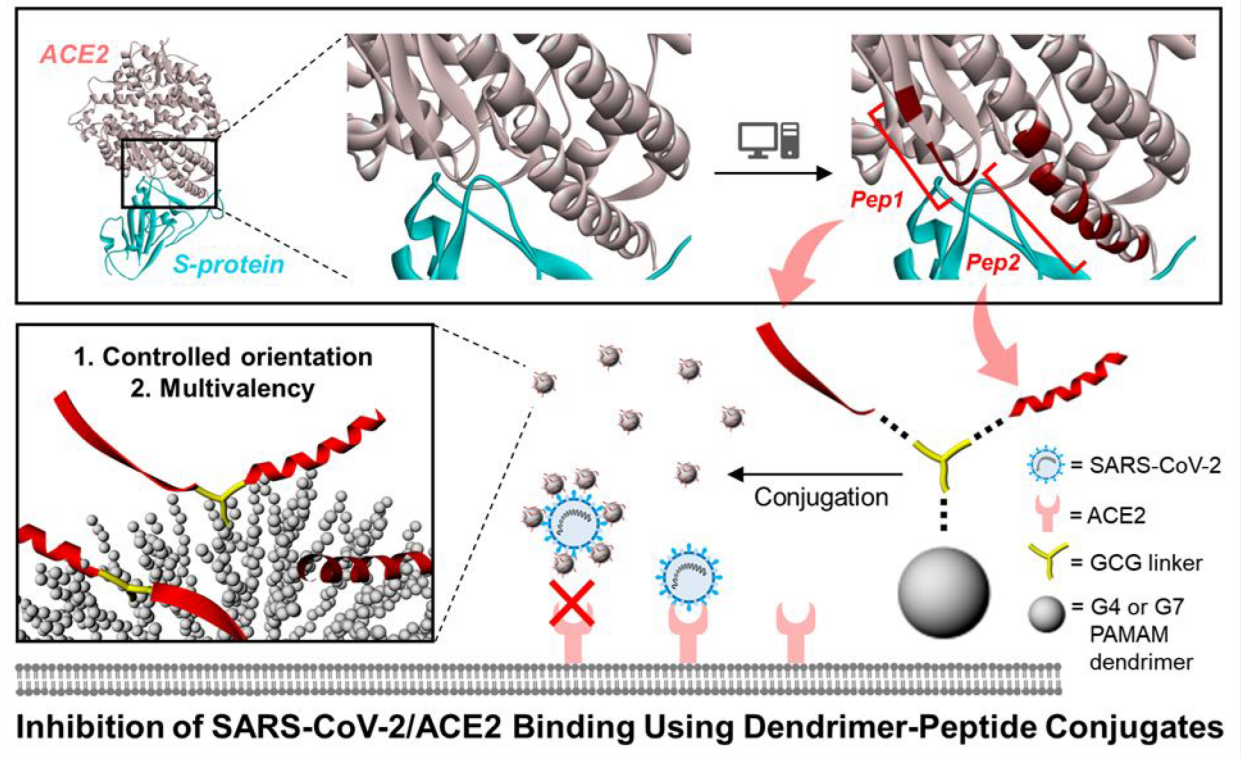

Figure 1. Inhibition of SARS-CoV-2/ACE2 (PDB ID: 2AJF) binding using dendrimer-peptide conjugates consisting of two peptides, a linker, and a dendrimer.

Various treatment strategies have emerged with the appearance of COVID-19, including conventional drug-based approaches, peptides,[13,14] sulfonated glyco-dendrimers,[15] monoclonal antibodies, plasma therapy, and mechanical ventilation.[16] Among drug-based treatment strategies, the nucleoside analog prodrug Remdesivir (GS-5734) has received much attention due to its remarkable antiviral effect for SARS-CoV-1 and MERS-CoV in preclinical trials and animal studies.[17,18] However, recent clinical results obtained from a large cohort of 330 patients in 30 different countries suggest that the drug appears to have no significant effect on COVID-19 mortality, contradicting previous findings.[19] Alternatively, oral antiviral drugs such as Paxlovid (nirmatrelvir/ritonavir) and Molnupiravir (Lagevrio) have been authorized for preventing mild to moderate COVID-19 from worsening. However, these oral medications interact badly with other concurrent medications which have the potential to cause serious adverse effects, such as impaired taste and high blood pressure.[19]

Several monoclonal antibody treatments have also obtained clinical attention to combat SARS-CoV-2.[20] SARS-CoV-2 utilizes spike glycoproteins (Spike proteins) on their envelope to interact with angiotensin-converting enzyme 2 (ACE2) receptors present on lung tissue.[20−23] The binding of Spike proteins to ACE2 receptors is recognized as the most critical step for the SARS-CoV-2 infection, promoting viral cell entry.[24−26] Most of the currently available monoclonal antibody medications, such as Bamlanivimab (LY-CoV555) and a combination of Casirivimab (REGN10933)/Imdevimab (REGN10987), prevent the interaction between the Spike protein and ACE2 receptors via blockade of the receptor-binding domain (RBD) on the Spike protein.[27−30] Although these antibody drugs also received Emergency Use Authorization from the FDA to treat mild-to-moderate COVID-19 patients,[31] their clinical benefits remain unclear to hospitalized patients.[32] Given that the currently available COVID-19 treatments are of varied efficacy, more focus is on the prevention of transmission through vaccination rather than the treatment of the virus itself.[33] Thus, there is a significant need for an effective treatment for COVID-19 patients.

Early modeling and experiments have revealed that individual ACE2-based peptides can efficiently bind to the Spike proteins of SARS-CoV-2.[13−15] For example, Pomplun et al. identified three peptide sequences that form high-affinity binding with RBD on the Spike proteins.[34] These peptides demonstrated high selectivity toward SARS-CoV-2-spike-RBD, demonstrating a potential use of peptides as a target molecule for SARS-CoV-2. Herein, we examined the use of engineered dendrimer-peptide conjugates (DPCs) for COVID-19 treatment. Previously, DPCs have demonstrated potent protein−protein interaction (PPI) inhibitory functions, high target affinity and selectivity, and enhanced bioavailability or pharmacokinetics compared to the free peptides.[35−37] Considering that S proteins form trimers and bind to ACE2 protein via multivalent binding, the utilization of DPCs for COVID-19 treatment is a promising strategy to develop strong inhibitors of S protein binding to ACE2 receptors. In this study, two peptide fragments of ACE2 were incorporated into a single sequence and conjugated to the surface of poly(amidoamine) (PAMAM) dendrimers, based on the assumption that the multivalent ACE2-mimicking peptides could effectively block the S protein−ACE2 interaction (Figure 1). We investigated the therapeutic potential of the DPC approach by exploring its S protein−ACE2 interaction with conventional antibodies. Further, we provide a resource for designing efficacious and cost-effective DPC-based SARS-CoV-2 target

https://doi.org/10.1021/acs.biomac.2c01018
Biomacromolecules 2023, 24, 141−149

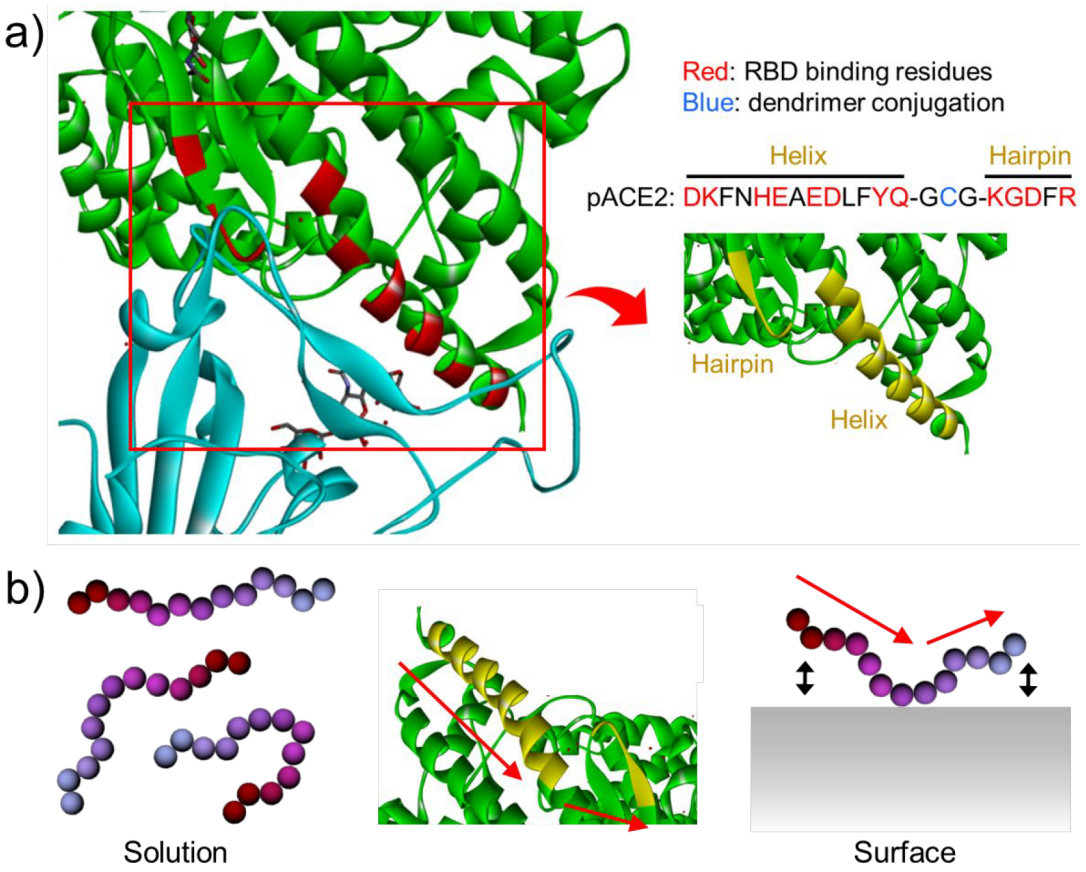

Figure 2. (a) The structure of synthesized S protein-binding peptide (pACE2) composed of the two sequences and a short linker. (b) Schematic illustration of the surface conjugation-mediated mimicry of molecular configuration of the ACE2 active site.

agents, which may have important implications for delivering antiviral payloads to SARS-CoV-2 with high affinity and selectivity.

EXPERIMENTAL SECTION

Cell Culture. Two human breast cancer cell lines, MDA-MB-231 and MCF-7, were used in this study. MDA-MB-231 and MCF-7 cells were cultured in Leibovitz's L-15 medium Dulbecco's modified eagle medium (DMEM), respectively, supplemented with 10% (v/v) FBS and 1% (v/v) P/S. Cells were cultured in a controlled humidified atmosphere with 5% CO_2 at 37 °C and grown in T-25 flasks until they reach 60−80% confluency.

Bead Preparation. The bead binding assay was performed to assess the blockade of S protein for each inhibitor. The carboxyl groups on fluorescently labeled beads (Bang Laboratories; 2×10^6 beads in 1 mL PBS) were activated using 1.8 mg/mL 1-(3-(Dimethylamino)propyl)-3-Ethylcarbodiimide Hydrochloride (EDC) and 2.8 mg/mL *N*-Hydroxy-Succinimide (NHS) (Sigma−Aldrich, St. Louis, MO). After 20 min EDC/NHS treatment, the beads were centrifuged for 3 min at 5,000g. Followed by 2 h incubation with 0.5 mg 5,000 MW carboxy-polyethylene glycol-amine (PEG; Nektar Therapeutics, Huntsville, AL). Unimmobilized PEG was then removed from the PEGylated beads using centrifugation (3 min, 5,000g, three times). PEGylated beads were functionalized with 5 μg/mL S protein using the same EDC/NHS chemistry. S ptotein-immobilized beads were then incubated with bovine serum albumin for 3 h to block the nonspecific bindings.

***In Vitro* Bead Binding Assay.** Cells were incubated in a 96-well plate and grown until they reach 80% confluency. The S protein-immobilized beads were incubated with different inhibitors for 30 min including free pACE2 peptides, the G4-pACE2 conjugates, the G7-pACE2 conjugates, and anti-SARS-CoV-2 antibodies, and each inhibitor was treated to the cells for 1 h in a serum-free media at the concentration of 10^4 particles per well in a 96-well plate. The number of beads bound to the cell surface was counted after three times of PBS washing.

Molecular Dynamics Simulation. The systems were simulated using NAMD 2.13[38,39] and the CHARMM36[40−42] protein force field. The simulations were conducted with the Langevin dynamics (γ_{ang} = 1 ps^{-1}) in the NpT ensemble, at a temperature of T = 310 K and a pressure of p = 1 bar. The particle-mesh Ewald (PME) method was used to evaluate Coulomb coupling, with periodic boundary conditions applied.[43] The time step was set to 2 fs. The long-range van der Waals and Coulombic coupling were evaluated every 1- and 2-time steps, respectively. After 200,000 steps of minimization, the solvent molecules were equilibrated for 4 ns, while the dendrimers and RBD were constrained using harmonic forces with a spring constant of 1 kcal $(mol\ Å)^{-1}$. Next, the systems were equilibrated in for 100 ns with the bottom residues on the S protein RBD constrained.

MMGB-SA Calculations. The molecular mechanics generalized Born-surface area (MMGB-SA) method[14,44,45] was used to estimate the free energies of binding between peptides and RBDs. The free energies were estimated from separate MMGB-SA calculations for three systems (binding amino acids, RBD, and the whole complex) in configurations extracted from the MD trajectories of the whole complex in the explicit solvent. The MMGB-SA free energies of the extracted configurations of the systems were calculated as

$$G_{tot} = E_{MM} + G_{solv-p} + G_{solv-np} - T\Delta S_{conf} \quad (1)$$

where E_{MM}, $G_{solv\text{-}p}$, $G_{solv\text{-}np}$, and $T\Delta S_{conf}$ are the sum of bonded and Lennard-Jones energy terms, the polar contribution to the solvation energy, the nonpolar contribution, and the conformational entropy, respectively. The E_{MM}, $G_{solv\text{-}p}$, and $G_{solv\text{-}np}$ terms were calculated using the NAMD 2.13[38,39] package generalized Born implicit solvent

https://doi.org/10.1021/acs.biomac.2c01018
Biomacromolecules 2023, 24, 141−149

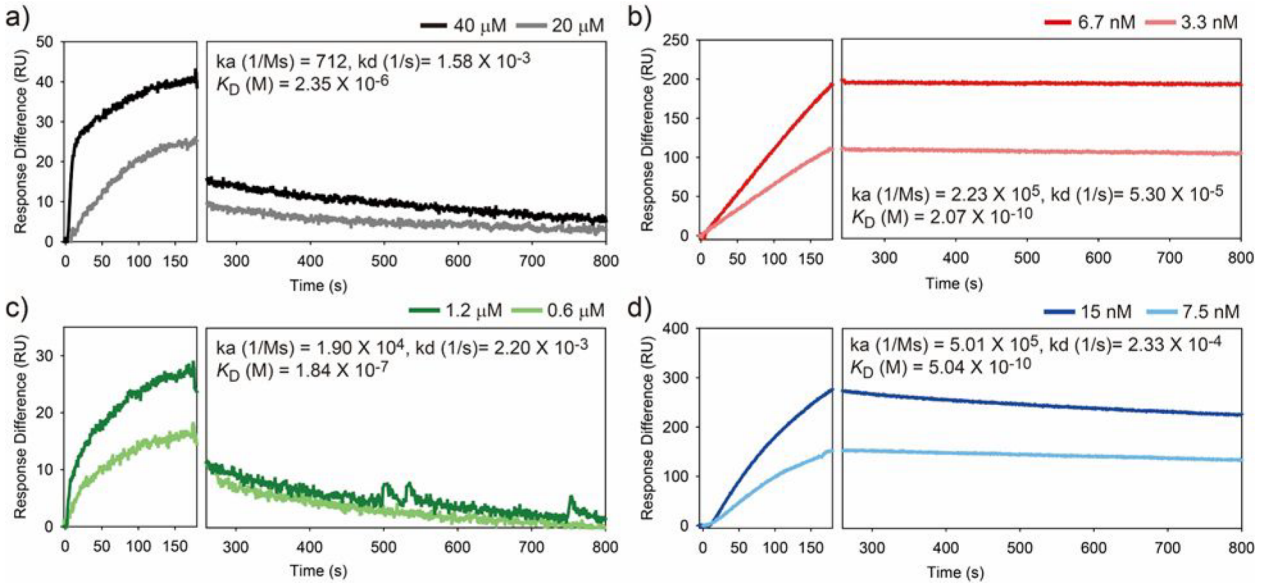

Figure 3. SPR sensorgrams for binding of (a) free pACE2, (b) anti-S protein antibody, (c) G4-pACE2, and (d) G7-pACE2 to S proteins.

model,[46] with the dielectric constant of water ε = 78.5. The $G_{solv\text{-}np}$ term for each system configuration was calculated in NAMD as a linear function of the solvent-accessible surface area (SASA), determined using a probe radius of 1.4 Å, as $G_{solv\text{-}np} = \gamma_{SASA}$, where γ = 0.00542 kcal mol^{-1} Å^{-2} is the surface tension. The ΔS_{conf} term was neglected since the entropic contribution nearly cancels when considering protein−protein binding of such similar structures. Since the G_{tot} values are obtained for peptide configurations extracted from the trajectories of complexes, G_{tot} does not include the free energies of peptide reorganization; the correct free energies of binding should consider configurations of separately relaxed systems. The approximate binding free energies of the studied complexes were calculated as

$$\langle \Delta G_{MMGB-SA} \rangle = \langle G_{tot}(\text{peptides} - \text{RBD}) - G_{tot}(\text{peptides}) - G_{tot}(\text{RBD}) \rangle \quad (2)$$

where peptides represent the chosen binding peptides, and the ⟨averaging⟩ is performed over configurations within the last 50 ns of the calculated trajectories.

RMSD Calculations. Time-dependent RMSD for the pACE2−1, pACE2−2, and pACE2−3 conjugated dendrimers were calculated from

$$\text{RMSD}_{\alpha}(t_j) = \sqrt{\frac{\sum_{\alpha=1}^{N_\alpha} \left| \vec{r}_\alpha(t_j) - \vec{r}_\alpha(t_0) \right|^2}{N_\alpha}} \quad (3)$$

where N_α is the number of atoms whose positions are being compared, $\vec{r}_\alpha(t_j)$ is the position of atom α at time t_j, and $\vec{r}_\alpha(t_0)$ is the initial coordinate.[47] The time-dependent RMSD was averaged over the last 50 ns of simulation time and is shown in Figure 5.

RESULTS AND DISCUSSION

In our previous study, it was found that the 15 amino acid residues of ACE2 play a critical role in the S protein binding.[13] Hence, considering that 13 of the residues are included in two short peptide fragments (KGDFR and DKFNHEAEDLFYQ) that are closely located in a small area (Figure 2a), we designed and synthesized a S protein-binding peptide (pACE2) composed of the two sequences and a short linker. A cysteine residue was introduced in the middle of the linker and used for the dendrimer conjugation, which allowed mimicking of spatial positions and orientations of the two peptide fragments in the ACE2 structure, as demonstrated in a previous study (Figure 2b). Therefore, the conjugation to the dendrimer surface enabled the peptides not only to form multivalent binding with S proteins but also to mimic the active site of ACE2, which could significantly enhance their target binding affinity as demonstrated in previous studies.[35,48,49]

SARS-CoV-2 spike protein-targeting dendrimer nanoparticles were prepared by the conjugation of approximately 4 and 40 pACE2 peptides to G4 (G4-pACE2 conjugates) and G7 PAMAM dendrimers (G7-pACE2 conjugates), respectively (Figures S2, S3, S4, and S5). Note that the number of peptides conjugated to each generation of dendrimers was determined to be less than 10% of the total primary amine groups. This would provide sufficient distance between the ligands and enable effective binding with the target molecules, as described previously.[35] Surface plasmon resonance (SPR) analysis indicated that the dendrimer-pACE2 conjugates bind more strongly with spike proteins than the free pACE2 peptides (Figure 3). The G4-pACE2 conjugates bound to spike proteins with a dissociation constant (K_D) of 1.84 × 10^{-1} μM which was 12.8-fold smaller than the K_D of free pACE2 peptides with spike proteins (2.35 μM). The increase in binding avidity was more prominent when pACE2 peptides were conjugated to the G7 PAMAM dendrimers. The binding avidity of the G7-pACE2 conjugates for spike proteins was 3 orders of magnitude stronger (K_D = 5.04 × 10^{-3} μM) than the free pACE2 peptides. On the other hand, the scrambled pACE2 peptides (pACE2_SC), G4-pACE2_SC, and G7-pACE2_SC showed little-to-no binding to the spike proteins (Figure S6). Specifically, a direct comparison of SPR sensograms revealed that the smaller K_D of the G7-pACE2 conjugates compared to that of the G4-pACE2 conjugates or free pACE2 peptides was attributed to both faster association and slower dissociation with the target molecules. Surprisingly, K_D of the G7-pACE2 conjugates was comparable to its whole antibody counterpart (anti-SARS-CoV-2 antibody) which binds to spike proteins with K_D of 2.07 × 10^{-3} μM. As circular dichroism (CD) analysis showed negligible conformational change in the peptides according to the conjugation (Figure S7), we

https://doi.org/10.1021/acs.biomac.2c01018
Biomacromolecules 2023, 24, 141−149

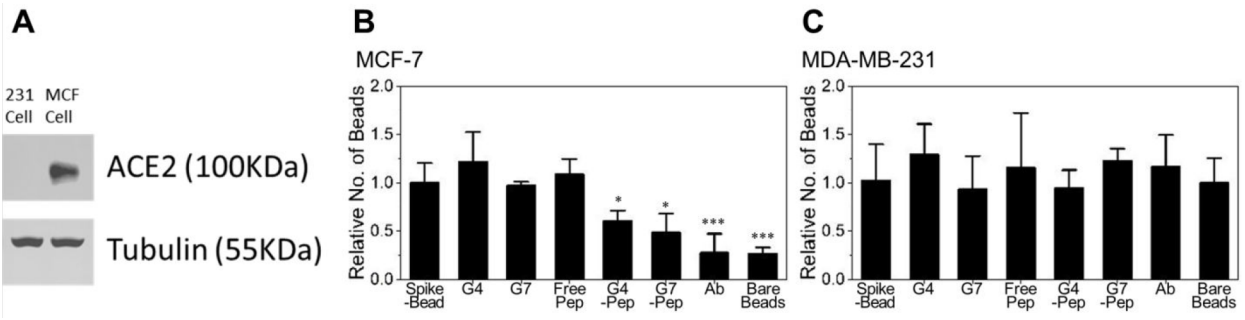

Figure 4. Inhibition between the ACE2 and SARS-CoV-2 spike proteins assessed *in vitro* using spike protein-coated fluorescent beads as a representative model for SARS-CoV-2. (a) Western blot analysis demonstrating the expression levels of ACE2 protein in MCF-7 and MDA-MB-231 cells. (b, c) The binding of spike protein-coated beads on MCF-7 and MDA-MB-231 cells after incubating the beads with either G4, G7, free pACE2, G4-pACE2, G7-pACE2, or antibodies for 1 h. Note that the statistical significance was analyzed compared to S protein-conjugated beads without any inhibitor treatments. Significance levels are indicated as $*p < 0.05$, $**p < 0.01$, and $***p < 0.001$, which are analyzed using Student's *t*-test.

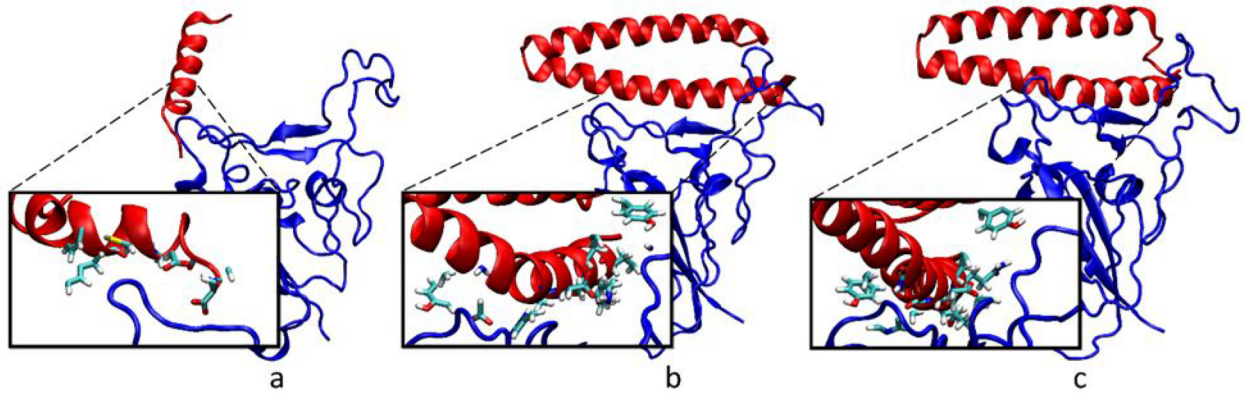

Figure 5. Binding of (a) pACE2−1, (b) pACE2−2, and (c) pACE2−3 free peptides to the RBD of the S protein of SARS-CoV-2. Red chains are the free peptides and blue chains are the RBD. Note that frames shown are 50 ns into the simulation.

speculated that the number of ligand molecules on the dendrimer surface highly affects the affinity to spike proteins that were densely packed on the SPR sensor chip. Also, considering that the trimeric spike protein is composed of three monomers with each having an RBD, the multivalent binding effect of the dendrimers enabled cooperative and strong interaction between RBD and pACE2 peptides, which eventually increased the binding avidity toward spike proteins.

The inhibition between the ACE2 and SARS-CoV-2 spike proteins was then assessed *in vitro* using spike protein-coated fluorescent beads as a representative model for SARS-CoV-2. Note that the size of the beads (10 μm) was larger than the actual SARS-CoV-2 virus. The beads were incubated with different inhibitors for 30 min including free pACE2 peptides, the G4-pACE2 conjugates, the G7-pACE2 conjugates, and anti-SARS-CoV-2 antibodies, and each inhibitor was treated to the cells for 1 h in a serum-free media at the concentration of 10^4 particles per well in a 96-well plate. As demonstrated in Figure 4, the G4-pACE2 conjugates effectively inhibited the interaction between the spike protein-coated beads and ACE2-expressing MCF-7 cells, resulting in a ∼39.3% reduced bead binding compared to the beads without any inhibitor treatment ($p = 0.047$). This was even more pronounced for the G7-pACE2 conjugates which showed an ∼51.4% reduced bead binding on MCF-7 cells ($p = 0.028$). In contrast, the free pACE2 peptides did not induce a noticeable difference with the nontreated controls, which implies that the inhibitory effect of the dendrimer-PACE2 conjugates is attributed to the enhanced binding kinetics of the conjugates to SARS-CoV-2 spike protein. However, the dendrimer-pACE2 conjugates were less effective than the anti-SARS-CoV-2 antibodies which demonstrated ∼73.3% reduction in bead binding, although the results were statistically insignificant ($p = 0.255$ for the G7-pACE2 conjugates vs anti-SARS-CoV-2 antibodies). This was contradictory to the results obtained from the SPR assay, as the G7-pACE2 conjugates were expected to exhibit a similar level of *in vitro* inhibitory effect to the antibodies. The lower *in vitro* efficiency of the G7-pACE2 conjugates compared to the SARS-CoV-2 antibodies is presumably due to the structural difference between the spike proteins on an actual virus and the microbead surface. The spike proteins on SARS-CoV-2 are comprised of a trimetric structure, while this structure is not maintained on the bead surface. Considering that the multivalent binding effect of the dendrimers would be more effective on trimetric structure, the dendrimer-pACE2 conjugates are expected to have a stronger inhibitory effect on an actual virus. It should also be noted that the free dendrimers or S protein beads without any inhibitor treatment did not induce a noticeable inhibitory effect on cells. Furthermore, the inhibitors used in this study had a minor effect on MDA-MB-231 cells which have low ACE2 expressions, demonstrating the selectivity of our dendrimer-pACE2 conjugates for targeting the spike proteins.

https://doi.org/10.1021/acs.biomac.2c01018
Biomacromolecules 2023, 24, 141−149

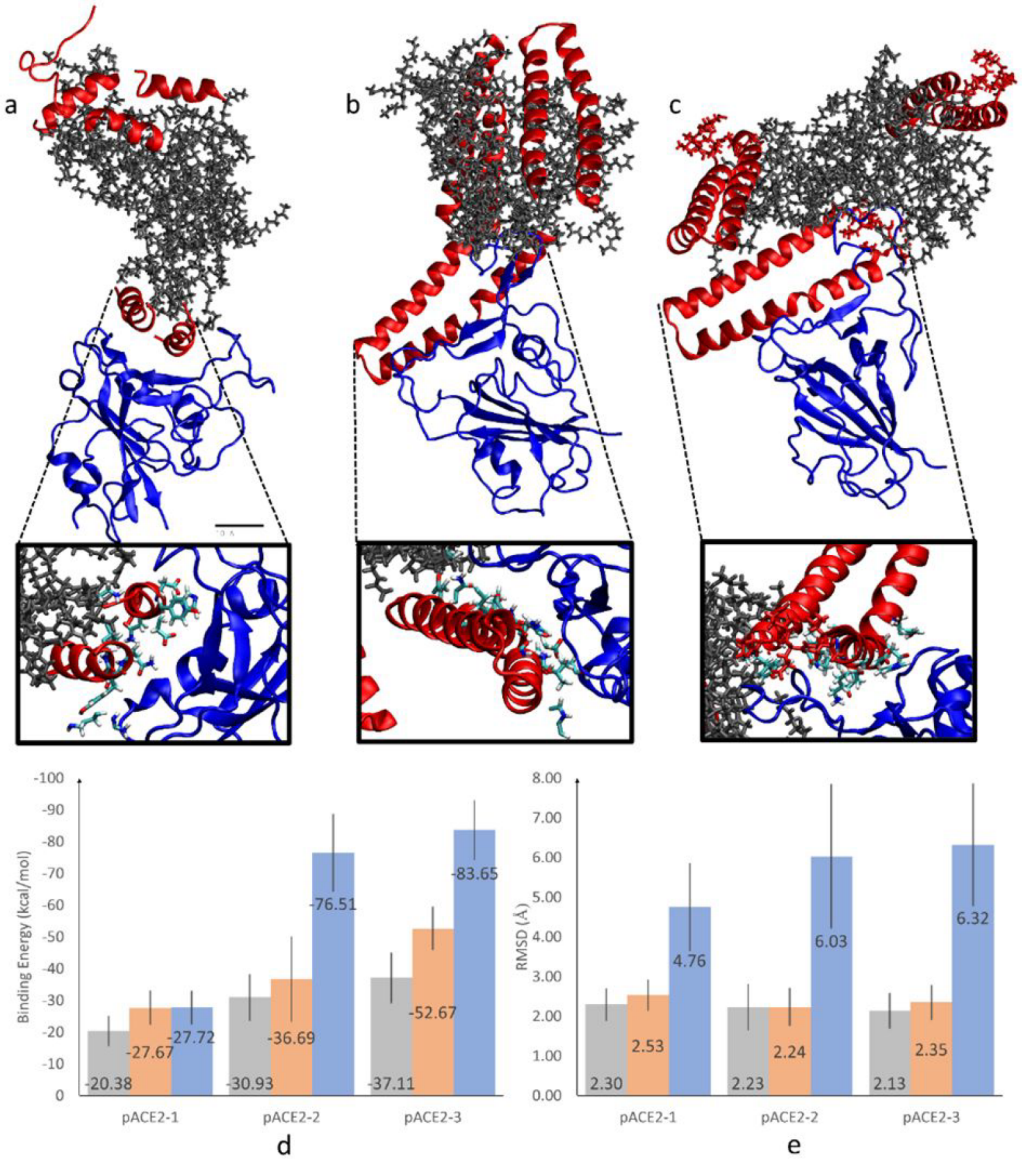

Figure 6. Binding of (a) pACE2−1, (b) pACE2−2, and (c) pACE2−3-conjugated generation 4 PAMAM dendrimers to the RBD of the S protein of SARS-CoV2 after 50 ns simulations. Red chains are conjugated peptides, gray chains are generation 4 PAMAM dendrimer, and blue chains are the RBD. (d) The free energy of binding between isolated and dendrimer-conjugated peptides and RBD. (e) The same as (d) for RMSDs. Gray − isolated peptides, orange − dendrimer-conjugated peptides, and blue − the entire peptide conjugated dendrimer and RBD complex. Note that MMGB-SA free energy and RMSD were calculated over final 50 ns of simulation.

In this study, we have demonstrated that pACE2 immobilized on PAMAM dendrimer surfaces block the binding of spike proteins to ACE proteins more effectively through a multivalent binding effect. Compared to free pACE2 peptides (negative controls), a high-density of reactive sites on the dendrimer surface allow for the conjugation of multiple peptides in a controlled distance. The flexible three-dimensional molecular structure of the PAMAM dendrimers then facilitates multiple interactions between peptides and spike proteins to occur in a single nanostructure. Molecular dynamics (MD) simulations of the studied systems were performed to better understand the experimental results, compare different dendrimer-peptide systems, and examine the benefits of the dendrimer-mediated multivalent binding effect.[13−15,50] A multivalent binding between peptide-conjugated dendrimers and the RBD of the Spike protein of SARS-CoV-2. Three peptides were tested for their binding to RBD: pACE2−1 (sequence DKFNHEAEDLFYQ-GCG-KGDFR), pACE2−2 (residues 22 to 88 in PDB 6M17, MET residue 88 mutated to CYS to link with sulfo-SMCC), and pACE2−3 (N-terminus and C-terminus of pACE2−2 bonded together). Six pACE2−1 and three pACE2−2/pACE2−3 were conjugated to a generation 4 PAMAM dendrimer via a sulfo-SMCC linker forming three conjugated dendrimers (pACE2−1-dendrimer, pACE2−2-dendrimer, and pACE2−3-dendrimer). The three conjugated dendrimers were subsequently placed above the RBD with one of the peptides binding to the RBD as in PDB 6M17. Figure 5 shows typical binding configurations for the individual peptides after 100 ns long MD simulations. All peptides remained in or near the binding position over the entire simulation trajectory.

Figure 6a−c shows typical binding configurations for the three conjugated dendrimers after 125.8, 100.2, and 123.8 ns long MD simulations, respectively. Each of the three systems

https://doi.org/10.1021/acs.biomac.2c01018
Biomacromolecules 2023, 24, 141−149

remained in a binding configuration throughout the whole simulation trajectory, where the peptides were close to their original configurations and conformations (folding). The peptides on the dendrimers also remained folded throughout the simulations, except pACE2−1. Figure 6d,e shows the free energies of binding and RMSDs, respectively, of the isolated and dendrimer-attached peptides. While pACE2−1 has a favorable free energy of binding, pACE2−2 and pACE2−3 have lower free energies and as such larger affinity with the RBD. For pACE2−1, almost all the free energy is derived from the binding peptides, which is not the case for pACE2−2 and pACE2−3. The dendrimer and nonbinding peptides contribute a sizable amount to the free energy in both, likely due to stabilization of the region binding with the RBD. We can also see that pACE2−1 has a higher but comparable RMSD of its binding peptides, while conjugated, than that of pACE2−2 and pACE2−3. All three proposed peptides have an average RMSD of less than 3 Å when binding with the Spike protein RBD. However, the RMSD of the free peptides is much higher for pACE2−1 than either pACE2−2 or pACE2−3, suggesting that it does not remain consistently tightly bound with the RBD.

CONCLUSION

It has been more than two years since the COVID-19 pandemic strongly impacted our lives. Despite the rapid development of various therapeutic options for COVID-19, the clinical outcomes of these early COVID-19 therapeutics were mostly disappointing. In this study, a novel SARS-CoV-2 antagonist was designed by the development of a peptide sequence (pACE2) which incorporated two different peptide fragments obtained from ACE2 protein, followed by the conjugation of these peptides to hyperbranched PAMAM dendrimers, in order to utilize the dendrimer-mediated multivalent binding effect. The SPR measurements revealed the enhanced binding interaction between pACE2 to SARS-CoV-2 spike proteins due to high generation PAMAM dendrimers. Specifically, the G7-pACE2 conjugates demonstrated 3 orders of magnitude stronger binding kinetics than the free pACE2, whereas the enhancement was only 12.8-fold for G4-pACE2. This clearly indicates that the dendrimer-mediated multivalent binding effect results in strong SARS-CoV-2 avidity. The *in vitro* assay using SARS-CoV-2-mimicking microbeads also demonstrated the effective blockade of binding between ACE2 and SARS-CoV-2 spike proteins for the dendrimer-pACE2 conjugates. The treatment of G4-pACE2 and G7-pACE2 conjugates to the SARS-CoV-2-mimicking microbeads resulted in 39.3% and 51.4% reduced binding to ACE2-positive MCF-7 cells, respectively. Furthermore, the interaction between the newly developed DPCs and SARS-CoV-2 was simulated using the MD method, providing an insight of how our DPC system enhances the SARS-CoV-2 blockade effect.

Some recent studies have demonstrated that SARS-CoV-2 may also infect tissues that do not express ACE2.[51] This report suggested that there are other mechanisms involved for the entry of SARS-CoV-2 other than the interaction between SARS-CoV-2-spike protein and ACE2 proteins. Although our study was focused on blocking the interactions between SARS-CoV-2 Spike protein and ACE2 proteins, our DPC systems can be further employed for inhibiting other receptors that may cause the entry of SARS-CoV-2 into cells. Previously, our team has shown that the dendrimer-mediated multivalent binding effect can facilitate the targeting of multiple proteins on the cell surface by co-conjugating peptides that target different cell surface proteins on the dendrimer surface.[37] Thus, other types of peptides that inhibit the entry of virus to the cells may be coimmobilized on our DPC system, which has potential to further prevent the SARS-CoV-2 infection. The therapeutic efficacy, bioavailability, and pharmacokinetics of our inhibitor will be the subject of our future studies that will focus on their *in vivo* behaviors. Nevertheless, the results presented in this study show that the dendrimer-mediated multivalent binding effect can enhance the SARS-CoV-2 antagonist effect, providing a novel potential antiviral drug delivery system for COVID-19, which could be potentially applied for other pandemic that may arise in the future.

ASSOCIATED CONTENT

Supporting Information

The Supporting Information is available free of charge at https://pubs.acs.org/doi/10.1021/acs.biomac.2c01018.

MALDI-TOF MS, CD, HPLC, ^{1}H NMR, TEM, DLS, and SPR data (PDF)

AUTHOR INFORMATION

Corresponding Authors

Heejoo Hong − *Department of Clinical Pharmacology & Therapeutics, Asan Medical Center, University of Ulsan, Songpa-gu, Seoul 05505, Korea*; Email: hhong@amc.seoul.kr

Petr Král − *Department of Chemistry and Department of Physics, University of Illinois at Chicago, Chicago, Illinois 60607, United States; Department of Pharmaceutical Sciences, University of Illinois at Chicago, Chicago, Illinois 60612, United States*; orcid.org/0000-0003-2992-9027; Email: pkral@uic.edu

Seungpyo Hong − *Pharmaceutical Sciences Division, Wisconsin Center for NanoBioSystems, and Lachman Institute for Pharmaceutical Development, The University of Wisconsin-Madison, Madison, Wisconsin 53705, United States; Department of Pharmaceutical Sciences, University of Illinois at Chicago, Chicago, Illinois 60612, United States; Yonsei Frontier Lab and Department of Pharmacy, Yonsei University, Seoul 03722, Korea*; orcid.org/0000-0001-9870-031X; Email: seungpyo.hong@wisc.edu

Authors

Woo-jin Jeong − *Pharmaceutical Sciences Division and Wisconsin Center for NanoBioSystems, The University of Wisconsin-Madison, Madison, Wisconsin 53705, United States; Department of Biological Sciences and Bioengineering, Inha University, Michuhol-gu, Incheon 22212, Korea*

Jiyoon Bu − *Pharmaceutical Sciences Division and Wisconsin Center for NanoBioSystems, The University of Wisconsin-Madison, Madison, Wisconsin 53705, United States; Department of Biological Sciences and Bioengineering, Inha University, Michuhol-gu, Incheon 22212, Korea*

Philip Mickel − *Department of Chemistry, University of Illinois at Chicago, Chicago, Illinois 60607, United States*

Yanxiao Han − *Department of Chemistry, University of Illinois at Chicago, Chicago, Illinois 60607, United States*

Piper A Rawding − *Pharmaceutical Sciences Division and Wisconsin Center for NanoBioSystems, The University of Wisconsin-Madison, Madison, Wisconsin 53705, United States*; orcid.org/0000-0002-9233-9700

Jianxin Wang − *Wisconsin Center for NanoBioSystems, The University of Wisconsin-Madison, Madison, Wisconsin 53705, United States*

Hanbit Kang − *Department of Biological Sciences and Bioengineering, Inha University, Michuhol-gu, Incheon 22212, Korea*

Complete contact information is available at: https://pubs.acs.org/10.1021/acs.biomac.2c01018

Author Contributions

#The manuscript was written through contributions of all authors. All authors have given approval to the final version of the manuscript. These authors contributed equally. W.-j.J. and J.B. contributed equally.

Funding

This study was partially supported by National Science Foundation (NSF) under grant # DMR-1808251 and 2211932. The authors also acknowledge the partial support from the Wisconsin Head & Neck Cancer SPORE Grant from NIH (P50-DE026787), The Falk Medical Research Trust − Catalyst and Transformational Awards Program, and Milton J. Henrichs Chair Funds. Partial support from the National Research Foundation of Korea (NRF) grant funded by the Ministry of Science and ICT (2021R1C1C1009912, 2021R1A4A3024237) is also acknowledged.

Notes

The authors declare no competing financial interest.

REFERENCES

(1) Gao, G. F. From "A"IV to "Z"IKV: Attacks from Emerging and Re-Emerging Pathogens. *Cell* **2018**, *172* (6), 1157−1159.

(2) Zhu, N.; Zhang, D.; Wang, W.; Li, X.; Yang, B.; Song, J.; Zhao, X.; Huang, B.; Shi, W.; Lu, R.; Niu, P.; Zhan, F.; Ma, X.; Wang, D.; Xu, W.; Wu, G.; Gao, G. F.; Tan, W. A Novel Coronavirus from Patients with Pneumonia in China, 2019. *N. Engl. J. Med.* **2020**, *382* (8), 727−733.

(3) Su, S.; Wong, G.; Shi, W.; Liu, J.; Lai, A. C. K.; Zhou, J.; Liu, W.; Bi, Y.; Gao, G. F. Epidemiology, Genetic Recombination, and Pathogenesis of Coronaviruses. *Trends Microbiol.* **2016**, *24* (6), 490−502.

(4) Zaki, A. M.; van Boheemen, S.; Bestebroer, T. M.; Osterhaus, A. D. M. E.; Fouchier, R. A. M. Isolation of a Novel Coronavirus from a Man with Pneumonia in Saudi Arabia. *N. Engl. J. Med.* **2012**, *367* (19), 1814−1820.

(5) Cui, J.; Li, F.; Shi, Z.-L. Origin and Evolution of Pathogenic Coronaviruses. *Nat. Rev. Microbiol.* **2019**, *17* (3), 181−192.

(6) Gorbalenya, A. E.; Baker, S. C.; Baric, R. S.; de Groot, R. J.; Drosten, C.; Gulyaeva, A. A.; Haagmans, B. L.; Lauber, C.; Leontovich, A. M.; Neuman, B. W.; Penzar, D.; Perlman, S.; Poon, L. L. M.; Samborskiy, D. V.; Sidorov, I. A.; Sola, I.; Ziebuhr, J.; Coronaviridae Study Group of the International Committee on Taxonomy of Viruses. The Species Severe Acute Respiratory Syndrome-Related Coronavirus : Classifying 2019-NCoV and Naming It SARS-CoV-2. *Nat. Microbiol.* **2020**, *5* (4), 536−544.

(7) Lu, R.; Zhao, X.; Li, J.; Niu, P.; Yang, B.; Wu, H.; Wang, W.; Song, H.; Huang, B.; Zhu, N.; Bi, Y.; Ma, X.; Zhan, F.; Wang, L.; Hu, T.; Zhou, H.; Hu, Z.; Zhou, W.; Zhao, L.; Chen, J.; Meng, Y.; Wang, J.; Lin, Y.; Yuan, J.; Xie, Z.; Ma, J.; Liu, W. J.; Wang, D.; Xu, W.; Holmes, E. C.; Gao, G. F.; Wu, G.; Chen, W.; Shi, W.; Tan, W. Genomic Characterisation and Epidemiology of 2019 Novel Coronavirus: Implications for Virus Origins and Receptor Binding. *Lancet* **2020**, *395* (10224), 565−574.

(8) Guan, W.; Ni, Z.; Hu, Y.; Liang, W.; Ou, C.; He, J.; Liu, L.; Shan, H.; Lei, C.; Hui, D. S. C.; Du, B.; Li, L.; Zeng, G.; Yuen, K.-Y.; Chen, R.; Tang, C.; Wang, T.; Chen, P.; Xiang, J.; Li, S.; Wang, J.; Liang, Z.; Peng, Y.; Wei, L.; Liu, Y.; Hu, Y.; Peng, P.; Wang, J.; Liu, J.; Chen, Z.; Li, G.; Zheng, Z.; Qiu, S.; Luo, J.; Ye, C.; Zhu, S.; Zhong, N. Clinical Characteristics of Coronavirus Disease 2019 in China. *N. Engl. J. Med.* **2020**, *382* (18), 1708−1720.

(9) Cucinotta, D.; Vanelli, M. WHO Declares COVID-19 a Pandemic. *Acta Biomed.* **2020**, *91* (1), 157−160.

(10) Kerr, C. C.; Mistry, D.; Stuart, R. M.; Rosenfeld, K.; Hart, G. R.; Núñez, R. C.; Cohen, J. A.; Selvaraj, P.; Abeysuriya, R. G.; Jastrzębski, M.; George, L.; Hagedorn, B.; Panovska-Griffiths, J.; Fagalde, M.; Duchin, J.; Famulare, M.; Klein, D. J. Controlling COVID-19 via Test-Trace-Quarantine. *Nat. Commun.* **2021**, *12* (1), 2993.

(11) Mathieu, E.; Ritchie, H.; Ortiz-Ospina, E.; Roser, M.; Hasell, J.; Appel, C.; Giattino, C.; Rodés-Guirao, L. A Global Database of COVID-19 Vaccinations. *Nature Human Behaviour* **2021**, *5*, 947.

(12) Dong, E.; Du, H.; Gardner, L. An Interactive Web-Based Dashboard to Track COVID-19 in Real Time. *Lancet Infect. Dis.* **2020**, *20* (5), 533−534.

(13) Han, Y.; Král, P. Computational Design of ACE2-Based Peptide Inhibitors of SARS-CoV-2. *ACS Nano* **2020**, *14* (4), 5143−5147.

(14) Chaturvedi, P.; Han, Y.; Král, P.; Vuković, L. Adaptive Evolution of Peptide Inhibitors for Mutating SARS-CoV-2. *Adv. Theory Simul.* **2020**, *3* (12), 2000156.

(15) Wells, L.; Vierra, C.; Hardman, J.; Han, Y.; Dimas, D.; Gwarada-Phillips, L. N.; Blackeye, R.; Eggers, D. K.; LaBranche, C. C.; Král, P.; McReynolds, K. D. Sulfoglycodendrimer Therapeutics for HIV-1 and SARS-CoV-2. *Adv. Ther (Weinh).* **2021**, *4* (4), 2000210.

(16) Gavriatopoulou, M.; Ntanasis-Stathopoulos, I.; Korompoki, E.; Fotiou, D.; Migkou, M.; Tzanninis, I.-G.; Psaltopoulou, T.; Kastritis, E.; Terpos, E.; Dimopoulos, M. A. Emerging Treatment Strategies for COVID-19 Infection. *Clin. Exp. Med.* **2021**, *21* (2), 167−179.

(17) Le Bras, A. Efficacy of Remdesivir in a Rhesus Macaque Model of MERS-CoV Infection. *Lab. Anim.* **2020**, *49* (5), 150−150.

(18) Sheahan, T. P.; Sims, A. C.; Leist, S. R.; Schäfer, A.; Won, J.; Brown, A. J.; Montgomery, S. A.; Hogg, A.; Babusis, D.; Clarke, M. O.; Spahn, J. E.; Bauer, L.; Sellers, S.; Porter, D.; Feng, J. Y.; Cihlar, T.; Jordan, R.; Denison, M. R.; Baric, R. S. Comparative Therapeutic Efficacy of Remdesivir and Combination Lopinavir, Ritonavir, and Interferon Beta against MERS-CoV. *Nat. Commun.* **2020**, *11* (1), 222.

(19) Bosilkovski, M.; Jakimovski, D.; Poposki, K.; Mateska, S.; Grujoski, M.; Dimzova, M. CURRENT SITUATION IN CHEMOPROPHYLAXIS AND THERAPEUTIC TREATMENT OF COVID-19. *Academic Medical Journal* **2022**, *2* (1), 4−12.

(20) Wu, Y.; Wang, F.; Shen, C.; Peng, W.; Li, D.; Zhao, C.; Li, Z.; Li, S.; Bi, Y.; Yang, Y.; Gong, Y.; Xiao, H.; Fan, Z.; Tan, S.; Wu, G.; Tan, W.; Lu, X.; Fan, C.; Wang, Q.; Liu, Y.; Zhang, C.; Qi, J.; Gao, G. F.; Gao, F.; Liu, L. A Noncompeting Pair of Human Neutralizing Antibodies Block COVID-19 Virus Binding to Its Receptor ACE2. *Sci.* **2020**, *368* (6496), 1274−1278.

(21) Letko, M.; Marzi, A.; Munster, V. Functional Assessment of Cell Entry and Receptor Usage for SARS-CoV-2 and Other Lineage B Betacoronaviruses. *Nat. Microbiol.* **2020**, *5* (4), 562−569.

(22) Surnar, B.; Kamran, M. Z.; Shah, A. S.; Dhar, S. Clinically Approved Antiviral Drug in an Orally Administrable Nanoparticle for COVID-19. *ACS Pharmacol. Transl. Sci.* **2020**, *3* (6), 1371−1380.

(23) Wrapp, D.; Wang, N.; Corbett, K. S.; Goldsmith, J. A.; Hsieh, C.-L.; Abiona, O.; Graham, B. S.; McLellan, J. S. Cryo-EM Structure of the 2019-NCoV Spike in the Prefusion Conformation. *Science* **2020**, *367*, 1260.

(24) Lan, J.; Ge, J.; Yu, J.; Shan, S.; Zhou, H.; Fan, S.; Zhang, Q.; Shi, X.; Wang, Q.; Zhang, L.; Wang, X. Structure of the SARS-CoV-2 Spike Receptor-Binding Domain Bound to the ACE2 Receptor. *Nat.* **2020**, *581* (7807), 215−220.

(25) Huang, K.-W.; Hsu, F.-F.; Qiu, J. T.; Chern, G.-J.; Lee, Y.-A.; Chang, C.-C.; Huang, Y.-T.; Sung, Y.-C.; Chiang, C.-C.; Huang, R.-L.; Lin, C.-C.; Dinh, T. K.; Huang, H.-C.; Shih, Y.-C.; Alson, D.; Lin, C.-Y.; Lin, Y.-C.; Chang, P.-C.; Lin, S.-Y.; Chen, Y. Highly Efficient and

Tumor-Selective Nanoparticles for Dual-Targeted Immunogene Therapy against Cancer. *Sci. Adv.* **2020**, *6* (3), eaax5032.
(26) Xia, S.; Zhu, Y.; Liu, M.; Lan, Q.; Xu, W.; Wu, Y.; Ying, T.; Liu, S.; Shi, Z.; Jiang, S.; Lu, L. Fusion Mechanism of 2019-NCoV and Fusion Inhibitors Targeting HR1 Domain in Spike Protein. *Cell. Mol. Immunol.* **2020**, *17* (7), 765−767.
(27) Robbiani, D. F.; Gaebler, C.; Muecksch, F.; Lorenzi, J. C. C.; Wang, Z.; Cho, A.; Agudelo, M.; Barnes, C. O.; Gazumyan, A.; Finkin, S.; Hagglof, T.; Oliveira, T. Y.; Viant, C.; Hurley, A.; Hoffmann, H.-H.; Millard, K. G.; Kost, R. G.; Cipolla, M.; Gordon, K.; Bianchini, F.; Chen, S. T.; Ramos, V.; Patel, R.; Dizon, J.; Shimeliovich, I.; Mendoza, P.; Hartweger, H.; Nogueira, L.; Pack, M.; Horowitz, J.; Schmidt, F.; Weisblum, Y.; Michailidis, E.; Ashbrook, A. W.; Waltari, E.; Pak, J. E.; Huey-Tubman, K. E.; Koranda, N.; Hoffman, P. R.; West, A. P.; Rice, C. M.; Hatziioannou, T.; Bjorkman, P. J.; Bieniasz, P. D.; Caskey, M.; Nussenzweig, M. C. Convergent Antibody Responses to SARS-CoV-2 Infection in Convalescent Individuals. *Nature* **2020**, *584*, 437−442.
(28) Shi, R.; Shan, C.; Duan, X.; Chen, Z.; Liu, P.; Song, J.; Song, T.; Bi, X.; Han, C.; Wu, L.; Gao, G.; Hu, X.; Zhang, Y.; Tong, Z.; Huang, W.; Liu, W. J.; Wu, G.; Zhang, B.; Wang, L.; Qi, J.; Feng, H.; Wang, F.-S.; Wang, Q.; Gao, G. F.; Yuan, Z.; Yan, J. A Human Neutralizing Antibody Targets the Receptor-Binding Site of SARS-CoV-2. *Nat.* **2020**, *584* (7819), 120−124.
(29) Chen, P.; Nirula, A.; Heller, B.; Gottlieb, R. L.; Boscia, J.; Morris, J.; Huhn, G.; Cardona, J.; Mocherla, B.; Stosor, V.; Shawa, I.; Adams, A. C.; Van Naarden, J.; Custer, K. L.; Shen, L.; Durante, M.; Oakley, G.; Schade, A. E.; Sabo, J.; Patel, D. R.; Klekotka, P.; Skovronsky, D. M. SARS-CoV-2 Neutralizing Antibody LY-CoV555 in Outpatients with Covid-19. *N. Engl. J. Med.* **2021**, *384* (3), 229−237.
(30) Weinreich, D. M.; Sivapalasingam, S.; Norton, T.; Ali, S.; Gao, H.; Bhore, R.; Musser, B. J.; Soo, Y.; Rofail, D.; Im, J.; Perry, C.; Pan, C.; Hosain, R.; Mahmood, A.; Davis, J. D.; Turner, K. C.; Hooper, A. T.; Hamilton, J. D.; Baum, A.; Kyratsous, C. A.; Kim, Y.; Cook, A.; Kampman, W.; Kohli, A.; Sachdeva, Y.; Graber, X.; Kowal, B.; DiCioccio, T.; Stahl, N.; Lipsich, L.; Braunstein, N.; Herman, G.; Yancopoulos, G. D. REGN-COV2, a Neutralizing Antibody Cocktail, in Outpatients with Covid-19. *N. Engl. J. Med.* **2021**, *384* (3), 238−251.
(31) Pardi, N.; Weissman, D. Development of Vaccines and Antivirals for Combating Viral Pandemics. *Nat. Biomed. Eng.* **2020**, *4* (12), 1128−1133.
(32) Sun, Y.; Ho, M. Emerging Antibody-Based Therapeutics against SARS-CoV-2 during the Global Pandemic. *Antibody Ther.* **2020**, *3* (4), 246−256.
(33) Salian, V. S.; Wright, J. A.; Vedell, P. T.; Nair, S.; Li, C.; Kandimalla, M.; Tang, X.; Carmona Porquera, E. M.; Kalari, K. R.; Kandimalla, K. K. COVID-19 Transmission, Current Treatment, and Future Therapeutic Strategies. *Mol. Pharmaceutics* **2021**, *18* (3), 754−771.
(34) Pomplun, S.; Jbara, M.; Quartararo, A. J.; Zhang, G.; Brown, J. S.; Lee, Y.-C.; Ye, X.; Hanna, S.; Pentelute, B. L. De Novo Discovery of High-Affinity Peptide Binders for the SARS-CoV-2 Spike Protein. *ACS Cent. Sci.* **2021**, *7* (1), 156−163.
(35) Jeong, W.-J.; Bu, J.; Han, Y.; Drelich, A. J.; Nair, A.; Král, P.; Hong, S. Nanoparticle Conjugation Stabilizes and Multimerizes β-Hairpin Peptides To Effectively Target PD-1/PD-L1 β-Sheet-Rich Interfaces. *J. Am. Chem. Soc.* **2020**, *142* (4), 1832−1837.
(36) Lau, J. L.; Dunn, M. K. Therapeutic Peptides: Historical Perspectives, Current Development Trends, and Future Directions. *Bioorg. Med. Chem.* **2018**, *26* (10), 2700−2707.
(37) Jeong, W.-J.; Bu, J.; Jafari, R.; Rehak, P.; Kubiatowicz, L. J.; Drelich, A. J.; Owen, R. H.; Nair, A.; Rawding, P. A.; Poellmann, M. J.; Hopkins, C. M.; Král, P.; Hong, S. Hierarchically Multivalent Peptide-Nanoparticle Architectures: A Systematic Approach to Engineer Surface Adhesion. *Adv. Sci. (Weinh).* **2022**, *9* (4), e2103098.
(38) Phillips, J. C.; Hardy, D. J.; Maia, J. D. C.; Stone, J. E.; Ribeiro, J. V.; Bernardi, R. C.; Buch, R.; Fiorin, G.; Hénin, J.; Jiang, W.; McGreevy, R.; Melo, M. C. R.; Radak, B. K.; Skeel, R. D.; Singharoy, A.; Wang, Y.; Roux, B.; Aksimentiev, A.; Luthey-Schulten, Z.; Kalé, L. V.; Schulten, K.; Chipot, C.; Tajkhorshid, E. Scalable Molecular Dynamics on CPU and GPU Architectures with NAMD. *J. Chem. Phys.* **2020**, *153* (4), 044130.
(39) Phillips, J. C.; Braun, R.; Wang, W.; Gumbart, J.; Tajkhorshid, E.; Villa, E.; Chipot, C.; Skeel, R. D.; Kalé, L.; Schulten, K. Scalable Molecular Dynamics with NAMD. *J. Comput. Chem.* **2005**, *26* (16), 1781−1802.
(40) Brooks, B. R.; Brooks, C. L.; Mackerell, A. D.; Nilsson, L.; Petrella, R. J.; Roux, B.; Won, Y.; Archontis, G.; Bartels, C.; Boresch, S.; Caflisch, A.; Caves, L.; Cui, Q.; Dinner, A. R.; Feig, M.; Fischer, S.; Gao, J.; Hodoscek, M.; Im, W.; Kuczera, K.; Lazaridis, T.; Ma, J.; Ovchinnikov, V.; Paci, E.; Pastor, R. W.; Post, C. B.; Pu, J. Z.; Schaefer, M.; Tidor, B.; Venable, R. M.; Woodcock, H. L.; Wu, X.; Yang, W.; York, D. M.; Karplus, M. CHARMM: The Biomolecular Simulation Program. *J. Comput. Chem.* **2009**, *30* (10), 1545−1614.
(41) Vanommeslaeghe, K.; Hatcher, E.; Acharya, C.; Kundu, S.; Zhong, S.; Shim, J.; Darian, E.; Guvench, O.; Lopes, P.; Vorobyov, I.; Mackerell, A. D. CHARMM General Force Field: A Force Field for Drug-like Molecules Compatible with the CHARMM All-Atom Additive Biological Force Fields. *J. Comput. Chem.* **2009**, *31*, 671−690.
(42) Yu, W.; He, X.; Vanommeslaeghe, K.; MacKerell, A. D. Extension of the CHARMM General Force Field to Sulfonyl-Containing Compounds and Its Utility in Biomolecular Simulations. *J. Comput. Chem.* **2012**, *33* (31), 2451−2468.
(43) Darden, T.; York, D.; Pedersen, L. Particle Mesh Ewald: An N·log(N) Method for Ewald Sums in Large Systems. *J. Chem. Phys.* **1993**, *98* (12), 10089−10092.
(44) Homeyer, N.; Gohlke, H. Free Energy Calculations by the Molecular Mechanics Poisson−Boltzmann Surface Area Method. *Mol. Inf.* **2012**, *31* (2), 114−122.
(45) Vergara-Jaque, A.; Comer, J.; Monsalve, L.; González-Nilo, F. D.; Sandoval, C. Computationally Efficient Methodology for Atomic-Level Characterization of Dendrimer−Drug Complexes: A Comparison of Amine- and Acetyl-Terminated PAMAM. *J. Phys. Chem. B* **2013**, *117* (22), 6801−6813.
(46) Tanner, D. E.; Chan, K.-Y.; Phillips, J. C.; Schulten, K. Parallel Generalized Born Implicit Solvent Calculations with NAMD. *J. Chem. Theory Comput.* **2011**, *7* (11), 3635−3642.
(47) Han, Y.; McReynolds, K. D.; Kral, P. Retrained Generic Antibodies Can Recognize SARS-CoV-2. *J. Phys. Chem. Lett.* **2021**, *12*, 1438.
(48) Jeong, W.; Choi, S.-H.; Jin, K. S.; Lim, Y. Tuning Oligovalent Biomacromolecular Interfaces Using Double-Layered α-Helical Coiled-Coil Nanoassemblies from Lariat-Type Building Blocks. *ACS Macro Lett.* **2016**, *5* (12), 1406−1410.
(49) Kim, J.-Y.; Lee, J. Y.; Park, H. Y.; Kim, H.; Kang, J. H.; Kim, H. J.; Jeong, W.-J. Combination of Peptides with Biological, Organic, and Inorganic Materials for Synergistically Enhanced Diagnostics and Therapeutics. *Pept. Sci.* **2022**, *114* (3), e24233.
(50) Sen, S.; Han, Y.; Rehak, P.; Vuković, L.; Král, P. Computational Studies of Micellar and Nanoparticle Nanomedicines. *Chem. Soc. Rev.* **2018**, *47* (11), 3849−3860.
(51) Puray-Chavez, M.; LaPak, K. M.; Schrank, T. P.; Elliott, J. L.; Bhatt, D. P.; Agajanian, M. J.; Jasuja, R.; Lawson, D. Q.; Davis, K.; Rothlauf, P. W.; Liu, Z.; Jo, H.; Lee, N.; Tenneti, K.; Eschbach, J. E.; Shema Mugisha, C.; Cousins, E. M.; Cloer, E. W.; Vuong, H. R.; VanBlargan, L. A.; Bailey, A. L.; Gilchuk, P.; Crowe, J. E.; Diamond, M. S.; Hayes, D. N.; Whelan, S. P. J.; Horani, A.; Brody, S. L.; Goldfarb, D.; Major, M. B.; Kutluay, S. B. Systematic Analysis of SARS-CoV-2 Infection of an ACE2-Negative Human Airway Cell. *Cell Rep* **2021**, *36* (2), 109364.

https://doi.org/10.1021/acs.biomac.2c01018
Biomacromolecules 2023, 24, 141−149